Generalized methodology for modeling and simulating optical interconnection networks using diffraction analysis

Ahmed Louri and Michael C. Major

Research in the field of free-space optical interconnection networks has reached a point where simulators and other design tools are desirable for reducing development costs and for improving design time. Previously proposed methodologies have only been applicable to simple systems. Our goal was to develop a simulation methodology capable of evaluating the performance characteristics for a variety of different free-space networks under a range of different configurations and operating states. The proposed methodology operates by first establishing the optical signal powers at various locations in the network. These powers are developed through the simulation by diffraction analysis of the light propagation through the network. After this evaluation, characteristics such as bit-error rate, signal-to-noise ratio, and system bandwidth are calculated. Further, the simultaneous evaluation of this process for a set of component misalignments provides a measure of the alignment tolerance of a design. We discuss this simulation process in detail as well as provide models for different optical interconnection network components.

Key words: Free-space optical simulation, optical interconnection networks, Fresnel diffraction, optical network modeling.

1. Introduction

Within the past few years, there has been a growing research trend in both the academic and the commercial arenas toward the employment of optical technology in computer interconnection networks.[1–11] This trend is fueled by the steady increase in the performance of modern computing systems and the corresponding demand for higher bandwidths from current interconnection networks. Faster computer components and newer, data-intensive computer architectures will require better interconnection systems to meet their performance capabilities. Research has already shown that optics technology offers advantages over electronics technology to provide these future interconnection solutions.[12–14]

Within the realm of optics, there exist several technologies capable of providing these interconnection systems. One technology revolves around the use of optical fibers and waveguides and already has a proven track record in the area of telecommunications.[1,4,7,15–17] Another technology uses free-space optics. Free-space optical systems offer several advantages for implementing interconnection networks. These advantages include the high parallelism of routing signals through a three-dimensional (3-D) volume, signal isolation, good power and thermal management, and low time skew between signals. These advantages motivated the research of free-space optical interconnection networks (OIN's).[3,11,18–26] This research has already expanded beyond theoretical considerations and into the realm of prototyping and constructing OIN's.[2,9,27–33]

As the volume of OIN research increases and the development of OIN's as commercial products begins, design tools will be necessary to quicken the design process, to identify problem areas, and to lower costs. Foremost of these tools will be simulation packages to permit exploration and refinements to OIN designs before the expensive implementation phase is entered. In particular, generic simulation packages capable of a variety of different optical systems would permit exploration of different OIN ideas without the creation of new simulators for each specific design.

The development of simulation methodologies to meet this growing need has so far been limited, and

The authors are with the Department of Electrical and Computer Engineering, The University of Arizona, Tucson, Arizona 85721.

Received 24 May 1994; revised manuscript received 3 November 1994.

0003-6935/95/204052-13$06.00/0.

the methodologies proposed so far have been restricted to simple systems.[34] Furthermore, these methodologies lack the capability of being applicable to a large range of different system designs while also permitting examination of the effects of minute changes, such as in component alignment and position. Our goal was to develop such a simulation methodology for a free-space system that would require only a description of the optical system (components, positions, alignment angles, etc.) and would allow the designer to simulate the system under a variety of different configurations and component alignments. We also sought to include active optical devices, such as spatial light modulators (self-effect electro-optic devices, liquid-crystal televisions, deformable mirrors, etc.), that could be used to perform switching in the network.

The focus of this paper is the presentation of a free-space OIN power simulation methodology capable of analyzing a variety of different network designs. In this simulation methodology, the simulator analyzes a description of the optical interconnect system of interest that is created by the designer. This network may contain active switching devices, and such networks are simulated with different switching configurations. The first stage of the analysis is the simulation of the light propagation through the network. This simulation is a two-step process. The first step of this process is a ray tracing of the optical channel of interest (which is defined by the user). This ray tracing provides information about the beam position and angle of incidence for each component in the system. This information is then used by the second step of the analysis, in which an electric field description of the light beam is propagated through the system. This propagation is simulated by the Fresnel diffraction equation. Furthermore, the use of diffraction analysis permits the propagation of electric subfields. By breaking the beam description into two subfields, each with an orthogonal polarity, one can simulate the polarity characteristics of the system as well. For the optical components, a combination of transmittance functions and Jones calculus[35] matrices is used in the modeling. This technique permits inclusion of both diffractive and refractive optics in the simulation as well as polarization-sensitive devices, which have not been shown in the other OIN simulation methodologies.[34]

The second stage of the analysis of the system provides the system characterization data. From the beam representations, optical signal power evaluations are performed through surface integration of the equivalent intensity fields. These evaluations include input optical power from the source plane, output optical power over the detectors, and optical cross-talk power. From these parameters the system metrics of optical efficiency, signal-to-noise ratio (SNR), and bit-error rate (BER) are determined. These parameters also calculate the maximum system bandwidth. Altogether, these metrics provide a measure of the performance capabilities of an OIN design. Furthermore, the proposed methodology permits the introduction of lateral and angular variances in the placement of components. The effect of these variances on the performance metrics provides a measure of the misalignment tolerance of the OIN system.

The rest of the paper is organized as follows. Section 2 discusses the OIN characteristics examined by this methodology. This section also provides the algorithm of the simulation methodology. Section 3 details the process of simulating the propagation of light by the use of the diffraction analysis method, and Section 4 explains the models used by the simulator for the various optical components found in OIN's. Section 5 examines our current research in developing an implementation of the algorithm. Section 6 concludes this paper.

2. Methodology for the Determination of Optical Interconnection Network Performance Characteristics

Here we present the basic methodology for the simulator. We begin by describing the network model to be used by the simulation methodology. This is followed by an examination of the performance characteristics calculated by the methodology. Finally, the methodology algorithm is presented.

A. Model for the Optical Interconnection Network

We now briefly discuss the OIN model for the proposed simulator methodology. The OIN is similar to electronic interconnects in that it comprises a collection of communication links between different computing nodes or components. In a free-space OIN, these links consist of arrays of light beams that fill a 3-D volume. The routing and control of these links are produced by a variety of different optical components such as lenses, prisms, and beam splitters. OIN's can also contain optical switching devices to change the routing of the various signal beams dynamically. Thus the OIN model consists of two planes within a 3-D volume, i.e., a source plane and a detector plane. Between these planes lie a series of blocks representing the beam-steering optics and the optical switches. The planes and blocks are connected together by links that represent the data channels of the network. Light travels in a single direction in this model (from the source plane to the detector plane); Fig. 1 shows the OIN model.

The goal of the presented simulation methodology is to calculate a set of metrics that measures a network's performance. These metrics are related to the signal power of the optical beams. Thus the details of the network model should be oriented for a technique of simulating light power flow. In the proposed methodology we use diffraction analysis for providing this simulation, and we discuss the reasons for choosing this method as well as the implementation of this technique in Section 3. Thus, with diffraction analysis, each of the component blocks consist of data planes. Each data plane contains

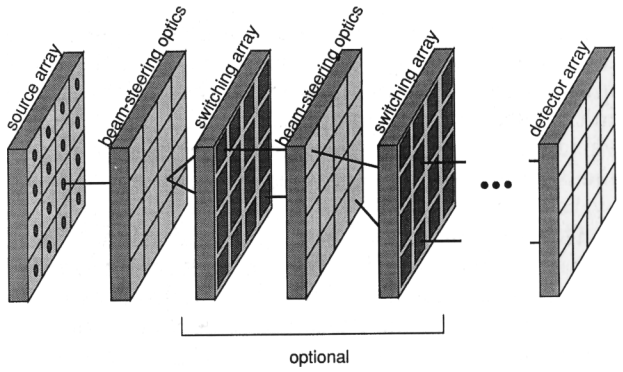

Fig. 1. Model for a 3-D OIN. An OIN consists of a two-dimensional array of signal beams routed between sources and detectors. Beam-steering optics between the sources and the detectors determine the topology of the OIN. Additionally, the network may include active switching components. Within the simulation framework, each component is represented by a two-dimensional data array.

sampled data that describe a small region of the component. These data consist of a transmittance function arranged into a Jones calculus matrix for inclusion of polarity effects. The diffraction analysis uses light information from each data plane to calculate the corresponding light field at the next data plane along the optical path.

B. Parameters Used in Simulation

As with any simulation, the methodology is dependent on the parameters desired from the simulation. These parameters may be divided into two sets: operation parameters and performance parameters. The operation parameters are values that can be physically measured from the network. With this methodology the primary operation parameters are based on the optical signal power. These parameters include the radiant source power, the irradiant detector power, and the optical cross-talk power. The performance parameters are metrics that define the capability and feasibility of the network. From these parameters we calculate the system performance metrics of optical system efficiency, SNR, BER, and network bandwidth. We discuss these parameters within the following subsections.

1. *Operation Parameters*

Because the operation parameters are quantities of optical power, the calculation of these parameters involves surface-integrating light intensity fields. These fields are only required at two locations: (a) immediately after the source plane and (b) immediately before the detector plane. Each intensity field is produced by[36]

$$I(x, y) = U_s^2(x, y) + U_p^2(x, y), \tag{1}$$

where U_s and U_p are the two electric light fields used by diffraction analysis. Within the intensity fields, the parameter being calculated defines the area of integration.

The first parameter of interest is the radiant power of the sources, $P_{\text{src\_signal}}$, which quantifies the amount of power in the data signal entering the network. Thus integration occurs over the source aperture on the source intensity field. The value of the parameter determines the amount of drive current necessary to modulate the light source. This information is needed for the design of the drive circuitry for the OIN sources and also influences some system properties such as heat dissipation, chip complexity, and the operating speed of the system.

The irradiant detector power or output power, $P_{\text{det\_signal}}$, requires an integration over the detector aperture area. This parameter defines the system operating speed and the feasibility of the design. If the output signal is too low, it will be indistinguishable from the detector noise and the network will not operate.

The optical cross-talk power, P_{ct}, is defined as the amount of overlap on the target detector from the other signal beams. Several methods exist to calculate this parameter, and the means used in this methodology is discussed in Subsection 2.C. This parameter provides a major factor to the system-noise calculations.

2. *Performance Parameters*

Optical efficiency (η_{sys}). The optical efficiency rates the power transfer capability of the OIN design. This metric is given by

$$\eta_{\text{sys}} = \frac{P_{\text{det\_signal}}}{P_{\text{src\_signal}}}. \tag{2}$$

Systems with low efficiency require higher-powered sources to provide a sufficient signal for the detectors. These systems are also more likely to have a higher ambient light level. This ambient light appears as a factor in the system noise.

System bandwidth (BW). The system bandwidth indicates the maximum data flow capable from the design. One obtains the bandwidth by first calculating the maximum data-transmission rate with

$$T_{\text{int}} = \frac{P_{\text{det\_signal}}}{E_{\text{detect}}}, \tag{3}$$

$$(R_{\text{trans}})_{\text{max}} = \frac{1}{T_{\text{int}}}, \tag{4}$$

where T_{int} is the integration time necessary to detect a single bit, E_{detect} is the threshold light energy for a logical one, and R_{trans} is the transmission rate. The data channel with the lowest R_{trans} sets the upper limit of the system's operating speed. One then determines the OIN bandwidth (BW) by

$$\text{BW} = MR_{\text{trans}}, \tag{5}$$

where M is the total number of data channels in the network.

This parameter is sensitive to the output power. A low output power results in a lower operating speed because of the longer integration times for the proper interpretation of the signal. Thus the system bandwidth is diminished. To correct this a designer must increase the input power, increase the system efficiency, or use more sensitive detectors. In each case the solution is expensive, and other factors often play a role as to which solution is taken. Improving the system efficiency carries the benefit of lowering heat dissipation, but it requires expensive alterations to the system. If diffraction is a major factor on system efficiency, larger apertures are necessary; this in turn could reduced bandwidth by reducing the number of channels in the system.

Signal-to-noise Ratio (SNR). The system reliability of an interconnect is often related by the system BER. The BER is defined as the probability for a given bit to be corrupted by the system.[37] For a digitial system this number must be kept very low, i.e., of the order of less than 10^{-17} for gigahertz transmission frequencies.[34] The BER is closely related to the system SNR. For an optical interconnect the SNR is found by

$$\mathrm{SNR} = \frac{P_{\mathrm{det\_signal}}}{P_{\mathrm{src\_noise}} + P_{\mathrm{sys\_noise}} + P_{\mathrm{det\_noise}}}. \tag{6}$$

System noise involves several factors, including cross talk and ambient light. Noise is also affected by component misalignment, aperture sizing, fluctuations in the light source, and electron noise in the detectors. Thus, to provide the low BER required for computing, a designer must strive to reduce all noise to the lowest possible level.

Bit-Error Rate (BER). There are several methods of calculating the BER of the optical interconnect.[34,37] One of the most robust methods involves the use of Gaussian statistics in the detection process. This leads to the following expression for the BER[34,38]:

$$\mathrm{BER} = \frac{1}{(2\pi Q)^{1/2}} \exp(-Q^2/2); \tag{7}$$

$$Q = \frac{|D - a_i|}{\sigma_i}, \tag{8}$$

D is the decision current threshold, i is the binary signal value, a_i is the signal current level, and σ_i is the variation in signal levels. Equations (7) and (8) are used to determine the optimum input power needed to achieve a given BER by[39]

$$P_{\mathrm{opt}} = \frac{1 + \mathrm{SNR}^{-1}}{1 - \mathrm{SNR}^{-1}} Q \frac{hc}{\lambda e} \langle i_{\mathrm{NA}}{}^2 \rangle^{1/2} \frac{N}{\eta_{\mathrm{tot}}}, \tag{9}$$

where h is Planck's constant, e is the charge of an electron, c is the speed of light, $\langle i_{\mathrm{NA}}{}^2 \rangle^{1/2}$ is the rms noise of the detector, η_{tot} is the total system efficiency including the detectors and sources, and N is the fan-out of the inputs.[34] Likewise, Eq. (9) may be rearranged to yield a value of Q:

$$Q = \frac{1 - \mathrm{SNR}^{-1}}{1 + \mathrm{SNR}^{-1}} \frac{\lambda e}{hc} \frac{1}{P_{\mathrm{opt}} \langle i_{\mathrm{NA}}{}^2 \rangle^{1/2}} \frac{\eta_{\mathrm{tot}}}{N}. \tag{10}$$

Equation (10) permits the calculation of the system BER for different values of input power.

Misalignment tolerance. Finally, OIN feasibility must be addressed by the designer, especially with regard to commercial implementation. To this end, misalignment tolerance must be examined. In manufacturing, systems must be assembled rapidly. Even with the use of robotics, positional and alignment variances will occur. Furthermore, temperature effects such as expansion and contraction will cause minute variations in position and alignment. A designer must be aware of these conditions and account for the effects of misalignment on system operation. Critical alignments may require special brackets and assembly procedures to be developed, which add to the system cost. Thus knowledge of such potential trouble areas is useful during the design process.

Misalignment does not relate with the other parameters with simple equations. For different OIN's, the relationship of misalignment to the other system parameters will vary substantially. Thus, for these misalignment relationships for a given OIN to be obtained, a recursive method of simulation with different misalignment values is necessary. This cyclic process then yields graphical representations of these misalignment relationships. These allow a designer to have a feel for the commercial suitability of the design. Designs whose operating characteristics are sensitive to alignment will be costly because of the need for extra stability in the design. These designs may also be impractical for certain operating environments.

C. Algorithm for the Determination of Performance Parameters

The initialization phase for this algorithm involves establishing the parameters that define the simulation environment. These parameters include a description of the OIN setup, information regarding the status of the optical switches, information about any misalignments to be implemented, and the signal channel to be analyzed. Initialization also retrieves the system description from a file created by another program such as a computer-aided design program, or one created by the designer. This file contains information regarding the types and configuration of the optical components. Further, component location and placement are included along with data about the number and types of sources and detectors.

We now describe the simulation algorithm. As we can see in Fig. 2, in step 1 the simulator loads the system description and then begins the primary loop, L1. Every cycle of this loop provides characteristic information of the OIN for a single switching state and a particular set of misalignments. Repeated cycles through this loop with changing misalign-

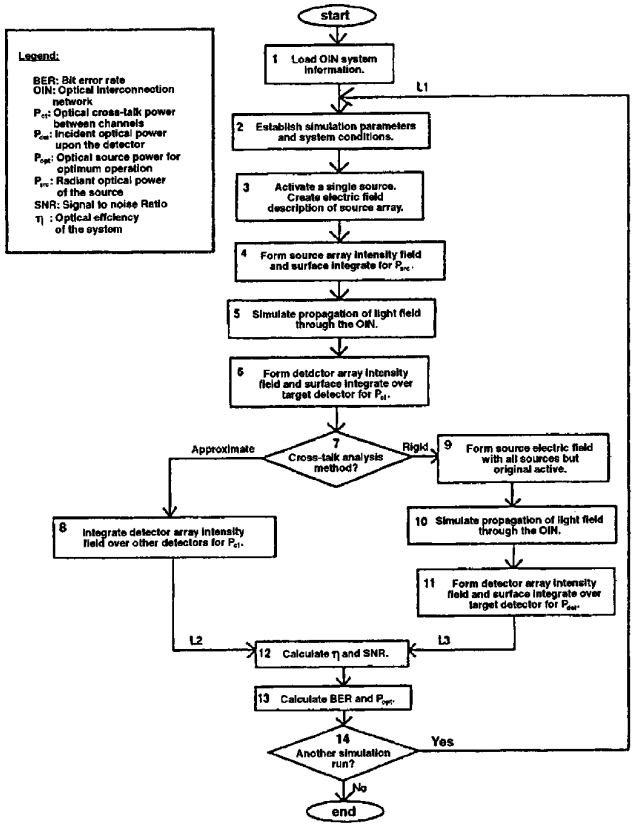

Fig. 2. Flowchart of the simulation methodology. The goal of this methodology is the interpretation of the power characteristics of an OIN. The methodology operates by taking information describing the optical system, establishing a single data channel to analyze, and propagating the electric field description of the light beam that makes up the data channel.

ments determine the misalignment characteristics of the OIN. The establishment of the switching state and misalignment information along with other system conditions and simulation parameters occurs immediately on entering the loop. From this information, a two-dimensional amplitude and phase description is formed for a light wave located immediately after the source array with only a single active source (which was chosen by the designer). An intensity field over the input array is formed from the description field and integrated over the aperture of the active source to determine the input power.

On calculation of the input power, the propagation of the electric light field through the OIN is simulated as shown in step 5. The details of this simulation are contained in Section 3. This propagation simulation forms an amplitude and phase description of the light wave incident upon the detector array. From this description, the calculation of an output intensity field proceeds in a similar manner to the previous formation of the input intensity field. Integration of the output field over the targeted detector aperture produces the output power.

The next task for the algorithm is the determination of the cross-talk power. There are two options available for this calculation. First, we can approximate the cross-talk power by surface integrating the current output intensity field over all of the nontargeted detectors and summing these results. This is shown in step 8. The basis of this approximation is the assumption that

$$P_{a/b} = P_{b/a},$$

where $P_{a/b}$ is the amount of optical power irradiant on detector a by a beam intended for detector b. This assumption depends on several factors. These factors are as follows.

First, the intensity profile of the beams must be symmetrical. This permits the intensity profiles over the two detectors to be symmetrical and the detected powers to be the same. However, in the case of an asymmetrical profile, the approximation method can still be valid if the targeted detector is the central detector of the array. Denoting this central detector as $D_{(0,0)}$, for every detector, $D_{(m,n)}$, we see that there exists a linearly symmetric detector, $D_{(-m,-n)}$. In this case,

$$P_{(m,n)/(0,0)} = P_{(0,0)/(-m,-n)}.$$

Thus,

$$P_{(m,n)/(0,0)} + P_{(-m,-n)/(0,0)} = P_{(0,0)/(m,n)} + P_{(0,0)/(-m,-n)},$$

and the total powers become equivalent.

Second, the placement of the beams should be uniform about the detector array. Inherent in the basic assumption is the requirement that the center of every beam be positioned similarly with respect to the center of each targeted detector. In other words, the location of the center of beam a on detector a is the same as the location of the center of beam b on detector b. Differences in these locations create differences in the amount of respective overlap from each beam and thus change the cross-talk power.

Third, the power in the different signal beams should be equivalent. If all the beams take paths through the same components, their powers should be equivalent. However, different beams may take different paths through the OIN system. These paths may have different optical efficiencies. If such is the case, the intensity of each output beam will vary and the approximation will be invalid. Similarly, the intensity profile between the data beams may be different, and this will also make the basic assumption false.

Although this approach is sensitive to changes in the optical system, the computational simplicity of the approach makes it attractive.

The second approach provides a more rigorous analysis. In this approach, shown as steps 9–11 in Fig. 12, the network is simulated again, but with the original source turned off and with the other sources activated. After the second simulation, a new output intensity field description is created and integrated over the original target detector for the cross-talk value. This is a much more computationally exhaustive method and still yields only an approxima-

tion. However, the method is not sensitive to the factors given in the previous approach and will produce more accuracy. In both approaches an input that maps with the central detector should be simulated to provide the highest cross-talk value. This would represent the worst-case signal for the network and would be the limiting factor on the OIN's SNR.

Once a value of cross talk is obtained, the simulation finishes with the calculation of the other system metrics. These metrics are obtained with the equations given above. The methodology is then repeated several times with varying levels of misalignment. The designer can plot the results to illustrate graphically the misalignment dependence of the OIN system.

3. Analysis of the Simulation of the Propagation of Light

A. Methodology for the Simulation of Light Propagation

For the simulation of an OIN, the optical system is described by an unfolded multistage representation. Figure 3 demonstrates this model. Each stage of the description consists of a single optical component and the free-space propagation region between the current component and the next component in the system, as shown in Fig. 4. As a result of the use of two orthogonally polarized electric light fields in the propagation routines, the components are described by transmittance functions arranged into Jones matrices. Jones calculus is employed to develop descriptions of the light field on the backside of the components for use by the diffraction equation. A discussion of the models for the various types of components used in an OIN is provided in Section 4.

Figure 5 is a flowchart of the methodology used for simulating propagation. The first step in the simulation methodology begins with the examination of the system state information, wherein the active inputs and switches are indicated. Field descriptions are then created for the active inputs with data from a system component description database. Next, an intensity field is calculated from this input field and integrated to derive a value of input light power. The simulator then enters a series of propagations from one component to the next. As mentioned above, the propagation is performed with the Fresnel diffraction equation with some help from a ray-trace

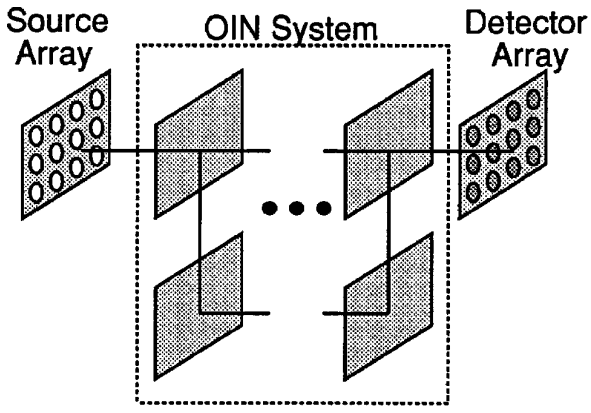

Fig. 3. Unfolded multistage representation of an OIN. This model consists of individual stages with a single component per stage. Components that receive the same multiple times are treated as multiple components.

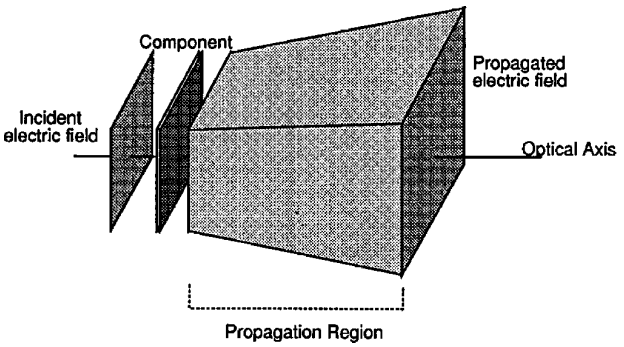

Fig. 4. Representation of a single stage in the OIN model. The primary components of a propagation stage are the incident light field, the component, and the free-space propagation region between the current component and the next component in the system.

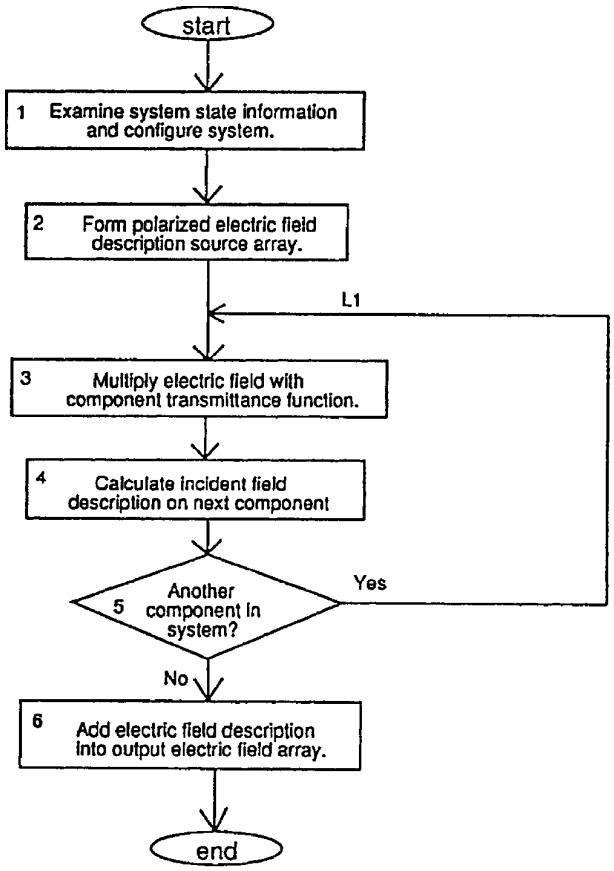

Fig. 5. Flowchart of the general approach for simulating the propagation of light. An electric field description of the light wave emitted from the source is created. This field description contains two subfields at orthogonal polarities to include polarity effects in the simulation. The field description is repetitively multiplied with a component's transmittance function and propagated to the next component until the description at the detector array is formed.

preprocessing step. At each component one multiplies the field description with the component transmittance description before proceeding with the next propagation. After propagation to the detector plane, the resultant field is converted into an intensity field for the estimation of values of output power, cross talk, or both.

Of note in Fig. 3 is the possibility of splitting the beam down two or more different paths. This is a common feature in many optical OIN's.[40] These splits are treated as separate and parallel stages in the network. However, this treatment is incomplete in itself. Often the light beam for each of these parallel stages has different characteristics than the beam in the other stages. For example, a polarizing beam splitter produces two beams with mutually orthogonal polarity, whereas a 50–50 beam splitter produces two beams that only differ by a π phase change. Thus, even though the component is the same in all these stages, the component transmittance function may be different and the components may be considered as different for modeling purposes. In this case the OIN model considers the beam split as having occurred before the beam splitter, which is modeled as two separate and parallel devices.

B. Implementation of Diffraction Analysis for Propagation

There are two approaches for evaluating the Fresnel diffraction equation,

$$U(x_0, y_0) = \frac{\exp(jkz)}{j\lambda z} \int_{-\infty}^{\infty} \int_{-\infty}^{\infty} U(x_i, y_i) \times \exp\left\{ j \frac{k}{2z} [(x_0 - x_i)^2 + (y_0 - y_i)^2] \right\} \mathrm{d}x_i \mathrm{d}y_i. \tag{11}$$

One approach involves the use of a surface-integration routine to calculate every sample point in a propagated field. The other technique involves the use of a two-dimensional fast Fourier transform (FFT) on the incoming electric field to form the propagated light field description. Both techniques offer benefits and limitations.

A mutual limitation on both techniques is the need for a sufficient number of sample points in the light field description to provide accurate results. With too few sample points, a condition of undersampling develops. In this situation the phase variation between two sampled points is greater than π, and the field is treated as having a different spatial frequency. The net result of this effect is the simulated propagation of a different light wave pattern. To prevent this, one should set the sampling frequency to at least twice the highest spatial frequency found in the system.[41]

This need for a large number of samples in the electric field has a direct impact on the execution speed of the simulation. The surface-integration routine has $O(n^2m^2)$ complexity, where n is the number of samples along one dimension in the input field and m is the number of samples along a single dimension in the propagated field. In comparison, the FFT has $O[n^2 \log(n)]$ complexity.[41] However, the FFT requires a zero-pad border to be added to the data field to avoid the data being interpreted as one cycle of a periodic function. This zero pad doubles the field size in each dimension.[41]

The FFT also has other limitations with the framework of the simulation methodology. One of these limitations is the need to preprocess the data field before the FFT is performed so that the resultant output field is not shifted. Another limitation is the dependence of the propagated field sample spacing on the propagation distance between stages. This spacing is also related to the sample spacing in the original data field. This relationship is given by

$$X_0 = N \frac{\lambda z}{X_i}, \tag{12}$$

where X_0 is the width of the output field, X_i is the width of the input field, N is the number of samples per dimension for both fields, λ is the operating wavelength, and z is the propagation distance. A result of this dependence is that control of the field size can only be maintained through the creation of a resized data field, where the samples are estimated from the samples of the FFT output field. The cost of this technique is loss of accuracy as well as additional computation time.

A third limitation of the FFT is the nature of the propagated description. This description is always centered around the optical axis of the system. Thus if a beam is located after propagation at a point far off the optical axis, the output field size must be sufficiently large to be able to include the beam. Because of the relationship mentioned above, this requires the input field to be substantially small or the number of samples to be significantly high. Both have an effect on the accuracy of the resultant field as well as the complexity of the calculation.

Because the surface-integration technique calculates values for specific output coordinates, the technique offers more flexibility than the FFT. With preknown knowledge of where beams are located through the system as well as estimates of the beam sizes, the integration technique avoids the additional limitations imposed on the FFT. Such beam-position knowledge can be gained through ray-tracing techniques. Thus, even though the integration technique is inherently more complex than the FFT technique, the additional calculations necessary to work around the FFT's limitations significantly reduces its speed advantage. For example, let us say that the input beam to a stage is 0.05 mm wide, is on the optical axis, and is described by 100 sample points in a 10×10 array. Ray tracing indicates that the beam on the output plane is displaced by 20 mm. The ray-trace–surface-integration approach can calcu-

late the beam description with only a 100 sample points over a 0.1 mm × 0.1 mm area in the region of the offset and store the offset value in an internal variable. In contrast, the FFT approach can only work on axis and requires the calculation of sample points over a 40.1 mm × 40.1 mm area (minimum). For the same sampling density as the surface-integration approach, this involves the calculation of 16,080,100 points. Thus the flexibility of the surface-integration approach can counter the computational complexity of the method and make the approach equivalent to the FFT approach with respect to the number of calculations.

For this methodology, the surface-integration approach is used to implement the diffraction analysis for propagating light. Associated with this analysis is a ray-trace preprocessing routine to identify the area for the integration routine to operate. As mentioned above, this will reduce the complexity of the calculation by the avoidance of calculations for areas where there is no signal.

Another point of concern are multiaxis devices such as lenslet arrays. For such devices each individual aperture contains its own optical axis. Normally a beam would be incident upon a single aperture, but in the event of misalignment the beam may cover more than one lenslet. In this situation each portion of the beam would be focused to each lenslet's focal point. For this to be simulated properly, each aperture must be propagated individually. The set of output fields created by this operation is then reconstructed into a unified field description. In this reconstruction, overlapping electric fields are summed together. This emulates the resulting interference that such overlaps create.

C. Algorithm for the Simulation of Light Propagation

Given the issue of the propagation of individual sources and apertures, as mentioned above, a highly iterative procedure is required. Figure 6 provides a detailed expansion of the general propagation simulation approach given in Fig. 5. The need to track individual inputs, beams, and apertures results in a series of nested loops. The outermost loop, L5, propagates the individual inputs. This is because diffraction analysis is only valid for coherent light. Although a single laser beam is coherent, light between beams from multiple lasers is incoherent. Diffraction analysis would incorrectly predict interference in this case.

Next, loop L4 is formed for the different beams created from a single input caused by beam splitters, diffraction gratings, and so on. Once split, these beams take different paths through the optical system, thus requiring the individual propagation of each beam. After this loop is established, the component description is examined. In the case of a component that produces multiple beams, the input field description is saved for use later in individually forming the different beams. Flags are examined

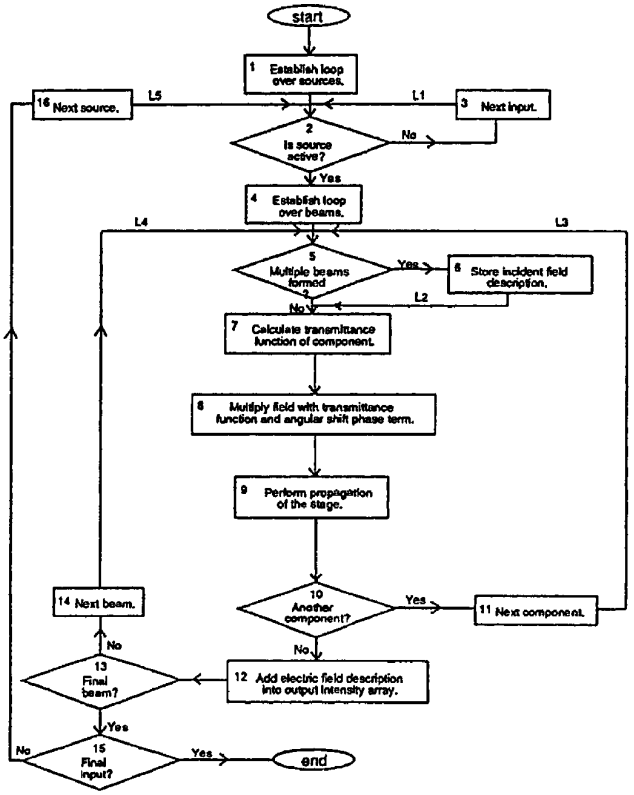

Fig. 6. Detailed flowchart of the propagation simulation methodology. Several loops are used to permit individual propagation of inputs and beams, with each beam propagated through the system on a component-by-component basis. After each beam reaches the detector array, it is added into a system output field description for use in calculating the system metrics.

and altered for each cycle of the beam loop to record which beams have already been propagated and which beam is next to be formed from the input description.

The component's transmittance function is now calculated and multiplied with the incident field description, as seen in steps 7 and 8 in Fig. 6. At this time, positional variances of the component are also taken into account. In the case of lateral shifts the electric field description is simply shifted by the appropriate amount. For an angular component alignment an additional calculation is required. Angular positional variances with respect to the light wave result in optical path-length differences, which in turn produce a phase variance across the light field but do not affect the polarity because the path is in a free-space environment. This phase variance is a function of the alignment angle, which is the angle of incidence with respect to the component normal made by the normal of the previous component. Through trigonometry the additional phase term is found to be $\exp(-jkx \tan(\theta))$, where θ is the alignment angle. Multiplication of this phase term with the electric field accounts for the angular alignment.

Finally, simulation of the light propagation is initiated as illustrated in Fig. 7. The simulator first determines the next component in the system and the

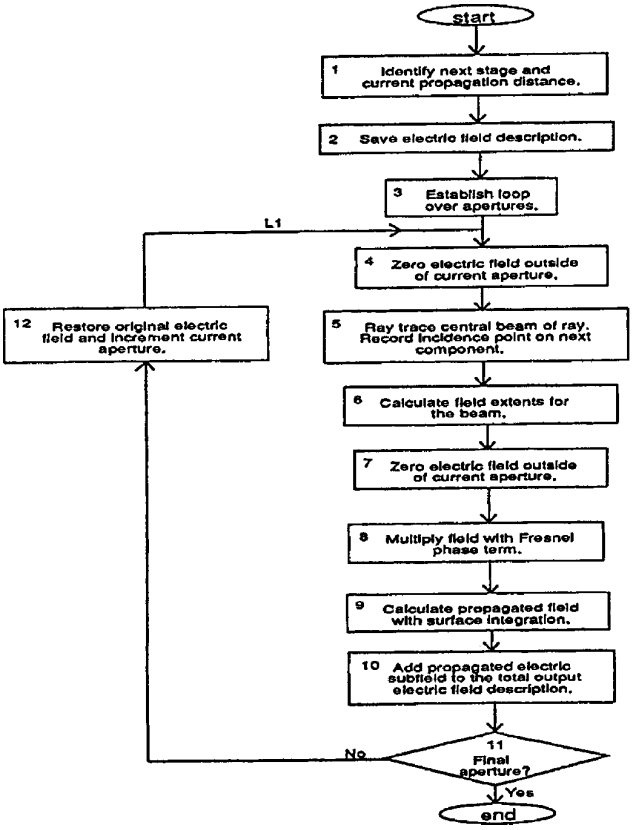

Fig. 7. Methodology for simulating the propagation of a light wave between components. The propagation is simulated for individual apertures in the component. For each propagation a ray trace is used to determine information on beam position; this is then used by the routines that perform the diffraction analysis, which involves surface integration of the Fresnel diffraction equation.

propagation distance. The loop over the different apertures of the current component is established. Next, a ray trace is performed for a ray at the center of the beam (or aperture). This ray trace determines the position of the incident beam on the next component. A Gaussian beam-size equation estimates the size of the propagated beam. An area that is a little larger than the estimated beam size is then established as the output beam area for the samples of the diffraction analysis. The section of the electric field covering the current aperture is isolated and multiplied with the Fresnel phase term. After this multiplication is performed, the surface integration routine is used for each of the sample points in the output field in loop L2. Interference effects from the other apertures are also summed into the sample values.

This propagation continues with all of the components in the signal path (loop L3). After having propagated a single beam to the detector plane, we begin step 14 and form an output intensity field from the electric field. This simply involves multiplying the values in the electric field with their complex complements. The detector intensity field is created from the different propagated beams through summation. This intensity field is then used for the calculation of the output and cross-talk powers. Once the final input has been propagated, the propagation routine is finished.

4. Component Models

As we mentioned above, optical components are represented by transmittance functions arranged into Jones matrices. To obtain these functions, we need models that are suitable for diffraction analysis. In this component modeling the descriptive equations or data fields for each type of component are developed for a fixed rotational orientation. Additional calculations are then employed to derive the transmittance functions of the components in other rotational positions. The first calculation determines the relative position of the sample points in the incident electric field array with respect to the fixed component. This maps the sample data points with the appropriate locations on the fixed position component description. In effect, the electric field is temporarily rotated to match the component description. The Jones matrix is formed with these relative position values. The Jones matrix is then adjusted to incorporate the component rotation. A Jones calculus rotation technique performs this adjustment. Through matrix multiplication, the desired transmittance matrix is found with

$$M_\theta = R_{-\theta} M_{\mathrm{std}} R_\theta; \tag{13}$$

$$R_\theta = \begin{bmatrix} \cos(\theta) & \sin(\theta) \\ -\sin(\theta) & \cos(\theta) \end{bmatrix}, \tag{14}$$

θ is the rotation angle, M_{std} is the standard position Jones matrix, and M_θ is the matrix at the desired rotation.[35] We now present the individual component models for many of the common components used in an optical interconnect. Many of these models, especially for the passive components, are simple extensions of models in common usage.

A. Lenses

One of the most common components in an OIN is the lens. Commonly in OIN's, lenses have been constructed into arrays for collimating light from the sources in the source array or for purposes of focusing onto the detector array. Lenses are also used occasionally for routing the light beams. From a diffraction standpoint, the lens operates by imparting either a spherical or a cylindrical phase alteration across the incident light wave. Figure 8 shows a basic lens with the appropriate measures for the model. The model for this lens is described as

$$t(x, y) = K \exp(jkn\Delta_0) \times \exp\left[-jk(n-1)\frac{x^2+y^2}{2}\left(\frac{1}{R_1}-\frac{1}{R_2}\right)\right], \tag{15}$$

where Δ_0 is the thickness of the lens at the center and

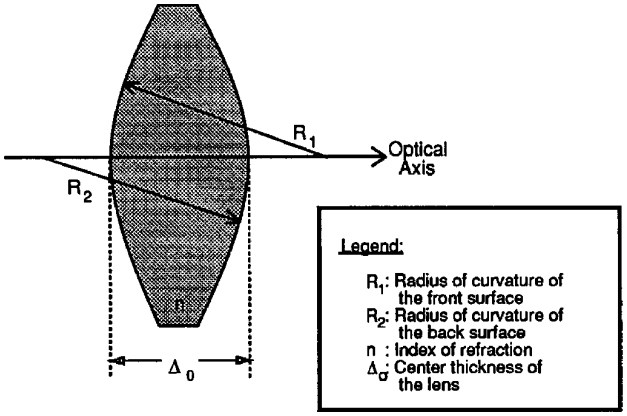

Fig. 8. Schematic for a basic thin lens that shows the measured parameters necessary for creating the lens model, which is dependent on the curvature of the front and back surfaces, the index of the lens, and the lens thickness.

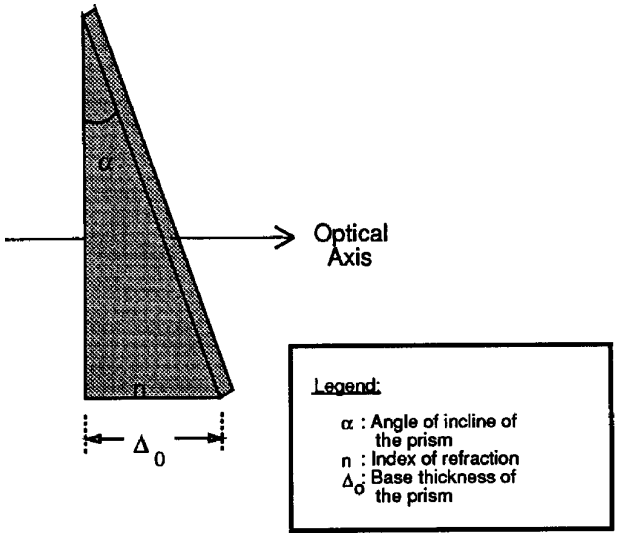

Fig. 9. Schematic of a thin prism. Indicated are the measured parameters necessary for creating the prism model, including the angle of incline of the prism, the index of refraction, and the prism base thickness.

R_i is the surface curvature measured from right to left.[36] Here K represents the amount of signal transmittance in the lens. A typical lens contains a 4% reflectance from each surface, which yields a K value of 0.922. However, if antireflective coatings are used, K approaches 1. By multiplying Eq. (15) with a 2×2 identity matrix, one creates the matrix model of the lens. In addition, in the case of a lenslet array, the values of x and y are referenced from the center of the respective lenslet in the array.

B. Thin Prisms

The behavior and model for the thin prism are similar to that of the lens. The prism behaves by altering the phase of the light wave front. The difference lies in the geometry of the phase change. Whereas the phase change from a lens is spherical, the phase change from a prism is linear. Thus the model equation for the prism becomes

$$t(x, y) = K \exp(jkn\Delta_0)\exp[-jk(n - 1)x \sin(\alpha)]. \quad (16)$$

As we can see in Fig. 9, α is the incline of the prism and Δ_0 is the thickness of the prism base. Differences in the orientation of the prism are handled through the rotation equations.

C. Diffraction Gratings and Holograms

Diffraction gratings and holograms behave similarly by imparting a pattern of phase or amplitude changes to an incident light wave. However, this pattern, especially in the case of the holograms, is rather complex. For these complex cases, either the descriptive transmittance function must be created by the designer or a descriptive file containing transmittance values in the proper array format must be provided to the simulator. For computer-generated holograms, this may be easily achieved by the conversion of the computer-generated hologram file into a format compatible with the simulator. For diffraction gratings with a simpile periodic pattern, such as a square wave or a sine wave, the equation approach is available for the creation of transmittance values. The patterns may be produced with either Eq. (17) for the amplitude grating or with Eq. (18) for the phase grating:

$$t(x, y) = K\left[\frac{1}{2} + \frac{a}{2} fn(x, f_0)\right], \quad (17)$$

$$t(x, y) = K \exp\left[j \frac{a}{2} fn(x, f_0)\right]. \quad (18)$$

In both equations a is the amplitude of the waveform, f_0 is the periodic frequency, and $fn(\ )$ is the waveform shape function. Currently the simulator is equipped with the descriptive equations for sine-wave and square-wave gratings.

D. Polarizers and Wave Plates

Polarizers and wave plates are optical components whose sole purpose is the alteration of the polarization of the light wave. As such, these components are well defined with Jones calculus. With the polarizer, the Jones matrix is

$$t = K\begin{bmatrix} 1 & 0 \\ 0 & 0 \end{bmatrix}. \quad (19)$$

Likewise, the wave plate is modeled as

$$t = K\begin{bmatrix} 1 & 0 \\ 0 & \exp(-j\Lambda) \end{bmatrix}, \quad (20)$$

where Λ determines the type of wave plate. For a quarter-wave plate, $\Lambda = \pi/2$, whereas $\Lambda = \pi$ for a half-wave plate.[35] Because these components alter

the entire wave front uniformly, no additional terms are necessary for the diffraction analysis. The diffractive effects caused by these components are due only to the apertures containing these components.

E. Spatial Light Modulators

The spatial light modulator (SLM) provides the switching capability for the OIN. Presented are models for two commonly used SLM's. One of these devices, the liquid-crystal television, is primarily a polarity-altering device that requires a Jones calculus approach in modeling. The model is complicated by the need to include a voltage term to alter the amount of change in the polarization. The Jones matrix of a liquid-crystal television with thickness d and that is twisted 90° is[42]

$$J = \exp(-j\phi) \times \begin{bmatrix} \left(\frac{\pi}{2\gamma}\right)\sin(\gamma) & \cos(\gamma) + j\left(\frac{\beta}{\gamma}\right)\sin(\gamma) \\ -\cos(\gamma) + j\left(\frac{\beta}{\gamma}\right)\sin(\gamma) & \left(\frac{\pi}{2\gamma}\right)\sin(\gamma) \end{bmatrix}, \tag{21}$$

where

$$\beta = \frac{\pi d}{\lambda}(n_e - n_o), \tag{22}$$

$$\phi = \frac{\pi d}{\lambda}(n_e - n_o), \tag{23}$$

$$\gamma = \left[\left(\frac{\pi}{2}\right)^2 + \beta^2\right]^{1/2}. \tag{24}$$

Under application of an electric field, a tilt angle is developed as given by

$$\theta = \begin{cases} 0 & V_{\mathrm{rms}} \le V_c, \\ \frac{\pi}{2} - 2\tan^{-1}\left\{\exp\left[-\left(\frac{V_{\mathrm{rms}} - V_c}{V_0}\right)\right]\right\} & V_{\mathrm{rms}} > V_c, \end{cases} \tag{25}$$

where V_c is the threshold voltage and V_0 is the excess voltage in which the tilt angle is 49.6° (see Ref. 42). Replacement of n_e with $n_e(\theta)$ is produced with

$$\frac{1}{n_e^2(\theta)} = \frac{\cos^2(\theta)}{n_e^2} + \frac{\sin^2(\theta)}{n_o^2}. \tag{26}$$

The symmetric self-effect electro-optic device is another SLM that has received much attention. To model this device the designer must determine the reflectance of the device in the on and off states. Phase change would also be measured. The device would then be represented by

$$t(x, y) = \begin{bmatrix} \rho\exp(j\phi) & 0 \\ 0 & \rho\exp(j\phi) \end{bmatrix}, \tag{27}$$

where ρ is the reflectance and ϕ is the phase change.

5. Implementation Status

We developed a rough implementation of the simulation algorithm in an effort to test the validity of this approach. The program provided adequate results for small systems (of the order of 4×4 and 8×8 matrices), but it placed a strain on our computing resources. One of the primary weaknesses in the implementation was the need for large blocks of memory. We used a conservative sampling approach in the rough implementation to avoid the problem of undersampling. The second weakness was the lengthy running times for each simulation with our limited computing resources (i.e., two Sun Sparc workstations and an IBM RS/6000).

Currently we are refining the simulation implementation to reduce or eliminate these weaknesses. To solve the memory problem, we are refining the sampling approach to have the simulator use just enough points to avoid undersampling while not sampling to the point that memory is wasted. An additional benefit of this research will be an increase in running speed, because the fewer number of samples corresponds to a lower number of calculations for the Fourier transform. To solve the running-time problem, we are exploring the alteration of the program code for use on a parallel machine. The algorithm contains many areas for potential parallelism. One of these areas is in the calculation of the output field. The calculation of each sample point in the output field is independent from the calculation of any other sample point in that field. Because these calculations form the bulk of the program's running time, parallelization of these calculations should show a considerable improvement in the program's running time. Such improvement is worth the effort in developing a parallel code.

6. Conclusions

The use of optics technology for computer interconnection networks has received much attention recently. The research of such networks has entered into the phase of the construction of prototypes, and the development of commercial systems is foreseeable in the near future. With this level of OIN design activity, there is currently a need for design tools to lower design time and cost. One necessary tool is an optical simulator to characterize network designs before the construction phase. Such a simulator would quicken the design process, identify problem areas, and lower research costs.

We presented a simulation methodology for the examination of free-space OIN's. With this methodology a broad range of OIN designs are capable of

being simulated. This simulation provides performance information with regard to the power flow of the light beams through the OIN, which in turn leads to the calculation of the performance parameters of signal-to-noise ratio, bit-error rate, and system bandwidth. Furthermore, the methodology permits the characterization of these parameters with varying degrees of component misalignment, thus providing a means to measure the misalignment tolerance of the OIN design.

The core of this methodology is the use of diffraction analysis technology to simulate the propagation of light through the OIN system. This type of analysis permits the simulator to be able to work with differences in source types as well as the myriad of different components that can make up an OIN. This is what permits the simulation methodology to operate with a variety of different networks. An additional flexibility of the diffraction analysis is the ability to propagate two fields with orthogonal polarizations independently. These two fields can be used to represent the actual electric field of the light beam. With this type of analysis, three characteristics of a light beam are simulated: amplitude, phase, and polarization. An implementation of the algorithm was developed. However, the implementation required a large amount of dedicated memory and took considerable time to run. Future research will involve optimization of this implementation to bring these problems to a reasonable level.

References

1. H. S. Hinton, "Architectural considerations for photonic switching networks," IEEE J. Sel. Areas Commun. **6,** 1209–1226 (1988).
2. L. Cheng and A. A. Sawchuk, "Three-dimensional omega networks for optical implementation," Appl. Opt. **31,** 5468–5479 (1992).
3. A. Louri and H. Sung, "Scalable optical hypercube-based interconnection network for massively parallel computing," Appl. Opt. **33,** 7588–7598 (1994).
4. T. S. Wailes and D. G. Meyer, "Multiple channel architecture: a new optical interconnection strategy for massively parallel computers," J. Lightwave Technol. **9,** 1702–1716 (1991).
5. U. Krackhardt, F. Sauer, W. Stork, and N. Streibl, "Concept for an optical bus-type interconnection network," Appl. Opt. **31,** 1730–1734 (1992).
6. A. Ghafoor, M. Guizani, and S. Sheikh, "Architecture of an all-optical circuit-switched multistage interconnection network," IEEE J. Sel. Areas Commun. **8,** 1595–1607 (1990).
7. J. W. Parker, "Optical interconnection for advanced processor systems: a review of the ESPRIT II OLIVES program," J. Lightwave Technol. **9,** 1764–1773 (1991).
8. N. C. Craft and A. Y. Feldblum, "Optical interconnects based on arrays of surface-emitting lasers and lenslets," Appl. Opt. **31,** 1735–1739 (1992).
9. T. Sakano, T. Matsumoto, K. Noguchi, and T. Sawabe, "Design and performance of a multiprocessor system employing board-to-board free-space optical interconnections: COSINE-1," Appl. Opt. **30,** 2334–2343 (1991).
10. A. Guha, J. Bristow, C. Sullivan, and A. Husain, "Optical interconnections for massively parallel architectures," Appl. Opt. **29,** 1077–1093 (1990).
11. A. Louri and H. Sung, "Efficient implementation methodology for three-dimensional space-invariant hypercube-based optical interconnection networks," Appl. Opt. **32,** 7200–7209 (1993).
12. R. A. Nordin, A. F. J. Levi, R. N. Nottenburg, J. O'Gorman, T. Tanbun-Ek, and R. A. Logan, "A systems perspective on digital interconnection technology," J. Lightwave Technol. **10,** 811–827 (1992).
13. M. R. Feldman, C. C. Guest, T. J. Drabik, and S. C. Esner, "Comparison between electrical and free space optical interconnects for fine grain processor arrays based on connection density capabilities," Appl. Opt. **28,** 3820–3829 (1989).
14. F. W. Kiamilev, P. Marchand, S. C. E. A. V. Krishnamoorthy, and S. H. Lee, "Performance comparison between optoelectronic and VLSI multistage interconnection networks," J. Lightwave Technol. **9,** 1674–1692 (1991).
15. M. G. Hluchyj and M. J. Karol, "ShuffleNet: an application of generalized perfect shuffles to multihop lightwave networks," J. Lightwave Technol. **9,** 1386–1397 (1991).
16. P. W. Dowd, "Wavelength division multiple access channel hypercube processor interconnection," "IEEE Trans. Comput. **41,** 1223–1241 (1992).
17. G. R. Hill, "Wavelength domain optical network techniques," Proc. IEEE **77,** 121–132 (1989).
18. F. B. McCormick and M. E. Prise, "Optical circuitry for free-space interconnections," Appl. Opt. **29,** 2013–2018 (1990).
19. T. J. Cloonan and F. B. McCormick, "Photonic switching applications of 2-D and 3-D crossover networks based on 2-input, 2-output switching nodes," Appl. Opt. **30,** 2309–2323 (1991).
20. M. G. Taylor and J. E. Midwinter, "Optically interconnected switching networks," J. Lightwave Technol. **9,** 791–798 (1991).
21. C. W. Stirk, R. A. Athale, and M. W. Haney, "Folded perfect shuffle optical processor," Appl. Opt. **27,** 202–203 (1988).
22. A. A. Sawchuk, C. S. Raghavandra, B. K. Jenkins, and A. Varma, "Optical crossbar networks," IEEE Trans. Comput. **20,** 50–62 (1987).
23. A. A. Sawchuk and T. C. Strand, "Digital optical computing," Proc. IEEE **72,** 758–779 (1984).
24. A. R. Dias, R. F. Kalman, J. W. Goodman, and A. A. Sawchuk, "Fiber-optic crossbar switch with broadcast capability," Opt. Eng. **27,** 955–960 (1988).
25. S. H. Song, E. H. Lee, C. D. Carey, D. R. Selviah, and J. E. Midwinter, "Planar optical implementation of crossover interconnects," Opt. Lett. **17,** 1253–1255 (1992).
26. J. M. Wang, L. Cheng, and A. A. Sawchuk, "Optical two-dimensional perfect shuffles based on a one-copy algorithm," Appl. Opt. **31,** 5464–5467 (1992).
27. K.-S. Huang, A. A. Sawchuck, B. K. Jenkins, P. Chavel, J.-M. Wang, and A. G. Weber, "Digital optical cellular image processor (DOCIP): experimental implementation," Appl. Opt. **32,** 166–173 (1993).
28. T. J. Cloonan, *Optical Computing Hardware* (Academic, San Diego, Calif., 1994), Chap. 1, pp. 1–43.
29. T. J. Cloonan, G. W. Richards, R. L. Morrison, F. B. McCormick, J. M. Sasian, A. L. Lenfine, S. J. Hinterlong, and H. S. Hinton, "Optically implemented shuffle equivalent interconnection topologies based on computer generated binary phase gratings," in *Photonics in Switching,* J. W. Goodman and R. D. Alferness, eds., vol. 16 of OSA Proceedings Series (Optical Society of America, Washington, D.C., 1993), pp. 147–151.
30. T. J. Cloonan and M. J. Herron, "Optical implementation and performance of one-dimensional and two-dimensional trimmed inverse augmented data manipulator networks for multiprocessor computer systems," Opt. Eng. **28,** 305–314 (1989).
31. K.-H. Brenner and A. Huang, "Optical implementations of the perfect shuffle interconnection," Appl. Opt. **27,** 135–137 (1988).
32. S. Lai and D. Hsu, "Perfect-shuffle implementation by using reflecting prisms," Appl. Opt. **31,** 6191–6192 (1992).

33. T. Sakano, K. Noguchi, and T. Matsumoto, "Multiprocessor system using an automatically rearrangeable free-space multichannel optical switch: COSINE-2," Appl. Opt. **32,** 3690–3699 (1993).
34. R. K. Kostuk, "Simulation of board-level free-space optical interconnects for electronic processing," Appl. Opt. **31,** 2438–2445 (1992).
35. B. E. H. Saleh and M. C. Teich, *Fundamentals of Photonics* (Wiley, New York, 1991).
36. J. W. Goodman, *Introduction to Fourier Optics* (McGraw-Hill, New York, 1968).
37. C. W. Stirk, "Bit error rate of optical logic: fan-in, threshold, and contrast," Appl. Opt. **31,** 5632–5641 (1992).
38. T. V. Muoi, "Receiver design for high-speed optical-fiber systems," J. Lightwave Technol. **LT-2,** 243–267 (1984).
39. H. Kressel and G. Arnold, *Semiconductor Devices for Optical Communication* (Springer-Verlag, New York, 1982).
40. T. J. Cloonan, G. W. Richards, A. L. Lentine, F. B. McCormick, H. S. Hinton, and S. J. Hinterlong, "A complexity analysis of smart pixel switching nodes for photonic extended generalized shuffle switching networks," IEEE J. Quantum Electron. **29,** 619–634 (1993).
41. R. D. Strum and D. E. Kirk, *Discrete Systems and Digital Signal Processing* (Addison-Wesley, Reading, Mass., 1989).
42. H.-K. Liu and T.-H. Chao, "Liquid crystal television spatial light modulators," Appl. Opt. **28,** 4772–4780 (1989).